Title
A Small Molecule Screen Identifies Selective Inhibitors of Urea Transporter UT-A

Journal
Cell Chemical Biology, 20(10)

ISSN
2451-9456

Authors
Esteva-Font, Cristina
Phuan, Puay-Wah
Anderson, Marc O
et al.

Publication Date
2013-10-01

DOI
10.1016/j.chembiol.2013.08.005

Peer reviewed

Published in final edited form as:
Chem Biol. 2013 October 24; 20(10): 1235–1244. doi:10.1016/j.chembiol.2013.08.005.

A SMALL MOLECULE SCREEN IDENTIFIES SELECTIVE INHIBITORS OF UREA TRANSPORTER UT-A

Cristina Esteva-Font[1], **Puay-Wah Phuan**[1], **Marc O. Anderson**[2], and **A.S. Verkman**[1]

[1]Departments of Medicine and Physiology, University of California, San Francisco CA, 94143-0521, U.S.A

[2]Department of Chemistry and Biochemistry, San Francisco State University, San Francisco CA, 94132-4136, U.S.A

SUMMARY

Urea transporter (UT) proteins, including UT-A in kidney tubule epithelia and UT-B in vasa recta microvessels, facilitate urinary concentrating function. A screen for UT-A inhibitors was developed in MDCK cells expressing UT-A1, water channel aquaporin-1, and YFP-H148Q/V163S. An inwardly directed urea gradient produces cell shrinking followed by UT-A1-dependent swelling, which was monitored by YFP-H148Q/V163S fluorescence. Screening of ~90,000 synthetic small molecules yielded four classes of UT-A1 inhibitors with low micromolar IC50 that fully and reversibly inhibited urea transport by a non-competitive mechanism. Structure-activity analysis of >400 analogs revealed UT-A1-selective and UT-A1/UT-B non-selective inhibitors. Docking computations based on homology models of UT-A1 suggested inhibitor binding sites. UT-A inhibitors may be useful as diuretics (‘urearetics’) with a novel mechanism of action that may be effective in fluid-retaining conditions in which conventional salt transport-blocking diuretics have limited efficacy.

INTRODUCTION

Urea is important in mammalian physiology, as it is the end-product of nitrogen metabolism and required for normal kidney function. The generation of a concentrated urine by the kidney involves a countercurrent multiplication mechanism, which is facilitated by aquaporins, a $Na^+/K^+/2Cl^-$ cotransporter (NKCC2) in the thick ascending limb of Henle, and urea transporters (UTs) in tubule epithelial cells and in microvascular (vasa recta) endothelia (Bankir and Yang, 2012; Fenton, 2009; Lei et al., 2011; Pannabecker, 2013; Sands 2007). Loss of UT function is predicted to disrupt urinary concentrating ability (Fenton et al., 2004; Sands and Layton, 2009), and hence UTs are potential targets for development of diuretics (‘urearetics’) with a novel mechanism of action and a unique clinical indication profile.

Kidney tubule epithelial cells express UT-A isoforms, encoded by the SLc14A2 gene; kidney microvascular endothelial cells (in vasa recta) express UT-B, encoded by the SLc14A1 gene (Bagnasco, 2003; Doran et al.; 2006, Fenton et al.; 2002, Shakayul et al.,

CONTACT: Alan S. Verkman, M.D., Ph.D., 1246 Health Sciences East Tower, University of California, San Francisco CA 94143-0521, USA; Phone 415-476-8530; Fax 415-665-3847; Alan.Verkman@ucsf.edu.

2013; Tsukaguchi et al., 1997). The UT-A gene family contains at least six isoforms, generated by alternative splicing, with the largest isoform being UT-A1 (Shakayul and Hediger, 2004; Smith, 2009; Stewart, 2011). UT-A1 and UT-A3 are expressed in kidney inner medullary collecting duct, and UT-A2 in thin descending limb of Henle in both inner and outer medulla (Fenton, 2009; Klein et al., 2012; Pannabecker, 2013; Sands, 2004). Knockout mice lacking both UT-A1 and UT-A3 manifest a marked urinary concentrating defect (Fenton et al., 2004, 2005; Fenton, 2008). However, urinary concentrating function is largely unimpaired in UT-A2 knockout mice (Uchida et al., 2005) and in UT-A1/A3 knockout mice after transgenic replacement of UT-A1 (Klein et al., 2013), suggesting UT-A1 as the principal UT-A-family target for inhibitor development. Knockout mice lacking UT-B (Yang et al., 2002; Yang and Verkman, 2002), and rare humans with loss of function mutations in UT-B (the erythrocyte JK antigen) manifest a relatively mild urinary concentrating defect (Lucien et al., 1998; Sands et al., 1992).

Until recently, available UT inhibitors included the non-selective membrane intercalating agent phloretin and millimolar-potency urea analogs (Mayrand and Levitt, 1983). Our lab identified nanomolar-affinity, small-molecule UT-B inhibitors using an erythrocyte lysis-based high-throughput screen (Levin et al., 2007). Erythrocytes express UT-B and are highly water permeable because they also express aquaporin-1 (AQP1) water channels. Erythrocyte lysis, as measured by infrared light absorbance, was used as a read-out of UT-B function following creation of an outwardly directed gradient of acetamide, a UT-B substrate with optimal transport properties for screening. Our original phenylsulfoxyoxozole UT-B inhibitors had IC_{50} ~100 nM for human UT-B, though they had much lower inhibition potency for rodent UT-B, precluding testing in rodent models (Anderson et al., 2012; Yao et al., 2012). A subsequent screen done using mouse erythrocytes identified triazolothienopyrimidines as UT-B inhibitors with IC_{50} ~ 25 nM for mouse UT-B and ~10 nM for human UT-B (Yao et al., 2012). The triazolothienopyrimidines had high selectivity for UT-B over UT-A, and they reduced urinary concentration in mice to that in UT-B knockout mice. However, the effect of UT-B inhibition or genetic deletion is modest – based on knockout mouse data and computational models UT-A is predicted to be substantially more important in urinary concentrating function. Recently, a thienoquinoline class of UT-B inhibitors was reported, albeit with relatively low inhibition potency (Li et al., 2013).

The purpose of this study was to identify UT-A1 inhibitors. We developed a robust cell-based high-throughput screen, which was applied to identify small molecule UT-A1 inhibitors. Following structure-activity analysis, compounds were identified with high UT-A1 selectivity, as well as non-selective compounds with similar UT-A1 and UT-B inhibition potency. Inhibition mechanisms were characterized and molecular docking computations were done to identify putative binding sites.

RESULTS

Development and validation of UT-A1 inhibitor screen

The UT-A1 assay developed for high-throughput screening involved measurement of cell volume changes in response to a rapidly imposed gradient of urea in MDCK cells stably expressing UT-A1 (Fig. 1A). Cell volume was followed using the chloride-sensing, genetically encoded fluorescent protein YFP-H148Q/V163S, which was developed previously for chloride channel screening (Galietta et al., 2001). Changes in cell volume alter intracellular chloride concentration, producing a near-instantaneous change in YFP fluorescence. The cells were also transfected with water channel AQP1 to ensure much higher water than urea permeability. Rapid addition of urea to the extracellular solution drives osmotic water efflux and cell shrinking, which is followed by urea (and water) entry

with return to the original cell volume. A urea concentration gradient of 800 mM was chosen empirically to produce a robust fluorescence signal for screening.

Original data from 96-well plates is shown in Fig. 1A (center), in which error bars indicate the minimal well-to-well variability. We found that UT-A1-facilitated urea transport in transfected MDCK cells grown on plastic did not require a cAMP agonist, in contrast to results for filter-grown, fully polarized MDCK cells (see below). Fig. 1B shows UT-A1 and AQP1 immunofluorescence, along with cytoplasmic YFP fluorescence in the transfected cells.

Data from cells transfected with YFP alone, and YFP together with UT-A1 and/or AQP1 are shown in Fig. 1C. Urea addition in the triply transfected cells (upper left) produced rapid cell shrinking and consequent reduced fluorescence, which was following by UT-A1-facilitated cell swelling and fluorescence increase. Inhibition by phloretin produced a greater initial fluorescence decrease and slowed recovery, similar to that in cells expressing YFP and AQP1 (without UT-A1, lower left). In the absence of AQP1 the phase of decreasing fluorescence was substantially slower (upper right), with UT-A1 reducing fluorescence signal because of the comparable rates of water and urea transport in these cells. The fluorescence decrease was slow and phloretin-independent in cells expressing YFP alone (lower right).

The assay was applied to test UT-A inhibition by two previously identified UT-B inhibitors, the phthalazinamine $urea_{inh}$-302 and the triazolothienopyrimidine UTB_{inh}-14. Fig. 1D shows dose-response data with IC_{50} for inhibition of UT-A1-facilitated urea transport of 16 μM for $urea_{inh}$-302, in agreement with 15 μM determined previously using a transepithelial transport assay (Levin et al., 2007). A very high concentration of UTB_{inh}-14 did not inhibit UT-A1-facilitated urea transport, in agreement with prior data showing very high UT-B selectivity (Yao et al., 2012).

Identification of UT-A1 inhibitors by high-throughput screening

The screening assay is diagrammed in Fig. 2A, in which cells were incubated with test compounds (25 μM) for 15 min at 37 °C, and then subjected to an 800-mM urea gradient during continuous measurement of YFP fluorescence. Fig. 2A (right) shows data from 10 individual wells for the negative control (DMSO vehicle alone) and positive control (phloretin). Robust differences were seen, with whole-plate Z′-factors generally greater than 0.55.

Fig. 2B provides examples of active and inactive compounds from the primary screen, showing compounds with ~0%, 50% and 100% inhibition. Fig. 2C shows the percentage inhibition of urea transport inhibition for 25,000 compounds from the primary screen, with the dashed line (at 90% inhibition) indicting the criterion to select active compounds. Results from a screen of 90,320 small synthetic compounds are summarized in Fig. 2D, which produced four distinct chemical classes of UT-A1 inhibitors, three of which (classes A, B and C, see below) are novel and one of which (class D) was identified previously in a UT-B inhibitor screen (Yao et al., 2012).

Structure-activity analysis of UT-A1 inhibitors

The structures of the most potent UT-A1 inhibitors emerging from structure-activity studies are shown in Fig. 3. A total of 106, 96, 27 and 200 commercially available analogs of class A, B, C and D inhibitors, respectively, were tested; data for the most potent compounds of each class are summarized in Table 1. Original concentration-inhibition curves are shown, in which increasing compound concentrations produce greater inhibition, with ~100% inhibition at high concentrations as judged by comparison with the phloretin data.

Compound selectivity for inhibition of UT-A1 vs. UT-B was studied. As diagrammed in Fig. 4A, a previously validated UT-B inhibition assay was used involving optical measurement of hypotonic lysis of acetamide-loaded erythrocytes following their rapid dilution into acetamide-free buffer (Levin et al., 2007). Fig. 4B shows dose-response data for UT-A1 and UT-B inhibition for the best UT-A1 inhibitors of each class. $UTA1_{inh}$-C1 showed high UT-A1 selectivity whereas $UTA1_{inh}$-B1 was non-selective. IC_{50} values for UT-A1 and UT-B inhibition are summarized in Table 1. Selectivity data for selected analogs are summarized in Fig. 4C. Interestingly, a large range of selectivities was found, even for the same compound class, with some compounds showing high UT-A1 or UT-B selectively, while others with little selectivity.

Structure-activity data for UT-A1 and UT-B inhibition provided information about the structural determinants for inhibitor activity. Fig. 4D summarizes the findings for class A inhibitors, the 8-hydroxyquinolines (8-HQ). Unsubstituted 8-HQ analogs (top panel) were UT-A1 selective. Their inhibition potency depended on the R^1 substituent, with benzylamine-bearing electron-donating group such as methoxy giving the best UT-A1 inhibition activity. Reduced activity was found with electron-withdrawing groups such as halides. Unsaturated cyclic rings (piperazines and cyclopentanamine) at R^1 also reduced inhibition activity. Aniline-substituted 8-HQ (bottom panel) were relatively non-selective, depending on the nature and position of the substituent on the aniline ring, with 3,4-di-substituted anilines with electron-donating and/or neutral substituent (such as methoxy, ethoxy or methyl) giving good UT-A1 inhibition. Mono-substitution with an alkoxy group at the 4-position on the aniline gave 8-HQs that inhibit both UT-A1 and UT-B (for example, $UTA1_{inh}$-A1 and $UTA1_{inh}$-A3 in Table 1). Br- and Cl-substituents on the aniline are tolerated, whereas di- or tri-substitutions on the aniline ring reduced activity.

UT-A1 inhibition mechanism

UT-A1 inhibition by compounds in each of the four classes was fully reversible. Cells were incubated with inhibitor for 15 min, washed, and assayed for UT-A inhibition. Inhibition was lost after washing (Fig. 5A).

The urea concentration dependence of UT-A1 inhibition was studied by inhibition measurements done using different urea concentrations. Fig. 5B (left) shows comparable percentage of UT-A1 inhibition for $UTA1_{inh}$-A1 using 800, 400 and 200 mM urea gradients. The deduced IC_{50} over a wide range of urea concentrations from 200–1600 mM (Fig. 5B, right) showed little effect of urea gradient size for $UTA1_{inh}$-A1, $UTA1_{inh}$-B1 and $UTA1_{inh}$-C1, indicating a non-competitive inhibition mechanism, and a ~2.5-fold increase in IC_{50} for $UTA1_{inh}$-D1, suggesting a competitive inhibition mechanism.

The kinetics of UT-A1 inhibition was determined by assay of UT-A1 inhibition at different times after compound addition. Fig. 5C (left) shows YFP fluorescence curves after addition of 3 μM $UTA1_{inh}$-B1 and $UTA1_{inh}$-C1, showing that inhibition by $UTA1_{inh}$-B1 occurred over minutes whereas $UTA1_{inh}$-C1 occurred within the time resolution of the measurement. Kinetic data for each compound are summarized in Fig. 5C (right). These results suggest an extracellular site of action for $UTA1_{inh}$-C1, and an intracellular site of action for the class A, B and D compounds. We previously reported that the UT-B selective class D analog UTB_{inh}-14 had an intracellular site of action in erythrocytes (Yao et al., 2012).

To verify UT-A1 inhibition using an independent assay that does not rely on water transport or fluorescent indicators, we measured UT-A1 facilitated urea transport in UT-A1-transfected MDCK cells on porous filters in which the kinetics of urea accumulation on the apical side was measured by enzymatic assay following addition of urea to the basal side of the filter (Fig. 5D). UT-A1 facilitated urea transport in this system required a cAMP agonist

forskolin and was inhibited by phloretin. Each of the compounds strongly inhibited UT-A1 urea transport.

Docking computations

Homology modeling and computational docking studies were done to investigate potential inhibitor binding sites and bound conformations. While a high resolution X-ray crystal structure of UT-A1 has not been reported, recently a structure of the homologous bovine UT-B bound to selenourea was solved at 2.5 Å (PDB=4EZD, Levin et al., 2012), allowing for the generation of a homology model of rat UT-A1. Potential inhibitor binding sites in the cytoplasmic and extracellular pore regions of UT-A1 were identified. Based on kinetic measurements in Fig. 5C, $UTA1_{inh}$-A1 and $UTA1_{inh}$-B1 were docked to the cytoplasmic pore region of UT-A1 (Figs. 6A,B), and $UTA1_{inh}$-C1 was docked to the extracellular pore (Fig. 6C). Ligand and protein preparation, as well as docking simulations, were performed with the OpenEye Scientific suite of utilities, including the software FRED (v2.2.5, McGann, 2011). In the bovine UT-B structure, two binding sites were identified for the urea analog selenourea (adjacent to Thr^{334} and Thr^{172}), which correspond to analogous sites in the central channel of our rat UT-A1 homology model. The cytoplasmic inhibitor binding site is surrounded by Leu^{652}, Leu^{895}, Glu^{572}, Ser^{700}, and Phe^{832}, while the extracellular inhibitor binding site is surrounded by Leu^{816}, Phe^{814}, Phe^{667}, Leu^{734}, Ala^{737}, and Pro^{808}. The majority of neighboring residues are hydrophobic, and the presence of Glu and Ser in the cytoplasmic binding site may provide an opportunity for structure-based optimization. While quantitative binding information based on homology models should be interpreted with caution, we note two results from the docking computations: *(a)* docking computations were successful in identifying the most active inhibitors (comparing to tested analogs) for each of class A, B, and D compounds; and *(b)* the predicted order of class B compounds (for UT-A1 inhibition potency) from computation agreed with experimental data. We did not attempt to model UT-A1 vs. UT-B selectivity because of limitations of homology models.

DISCUSSION

A screening assay was implemented to identify small-molecule UT-A1 inhibitors. Several classes of UT-A1 inhibitors were discovered with distinct chemical scaffolds, each of which yielded multiple active compounds. Interestingly, analogs were identified with high selectivity for inhibition of UT-A1 versus the other major renal urea transporter, UT-B, as well as analogs lacking selectivity. UT-A1 inhibition by all compounds was reversible; inhibition by class A, B and C compounds was non-competitive with urea, whereas inhibition by class D compounds was competitive. Functional studies, together with homology modeling and docking computations, suggested inhibitor binding sites for class A and B compounds near the intracellular urea pore region, and class C compounds near the extracellular pore region.

The screening assay utilized an epithelial cell line with intrinsically low urea permeability that grew rapidly on uncoated plastic and could be stably transfected to express UT-A1, AQP1 and YFP-H148Q/V163S. The constitutive activity of UT-A1 without the need for cAMP agonists was advantageous for high-throughput screening, as it reduced assay complexity. Transfection with AQP1 ensured that water permeability was much greater than urea permeability, which avoided potentially confounding compound effects on water permeability or cell volume, and which maximized the UT-A1-dependent difference in kinetic signal. Transfection with YFP-H148Q/V163S allowed for kinetic plate reader-based measurements of cell fluorescence, which was related to cell volume, as cell volume changes alter cytoplasmic chloride concentration reciprocally, changing YFP-H148Q/V163S fluorescence on a millisecond time-scale (Galietta et al., 2001). The intrinsic cell

fluorescence avoided the need for dye loading. A potential limitation of this assay is that YFP-H148Q/V163S fluorescence is sensitive to chloride concentration and pH; however, UT-A1-dependent changes in cell volume, which occur in seconds, are much faster than potential changes in chloride concentration and pH that may occur in response to secondary changes in electrochemical driving forces for chloride and proton transport. Notwithstanding this caveat, the assay was robust, technically simple and inexpensive, and successful in identifying small-molecule UT-A1 inhibitors.

Each of the four chemical classes has drug-like properties, including the presence of multiple hydrogen bond acceptors, as well as favorable molecular weight, aLogP and topological polar surface areas. The average molecular weights are 394, 343, 320 and 458 for active class A, B, C and D inhibitors, respectively; average aLogP values are 4.6, 1.9, 4.8, and 3.8; and average topological polar surface areas are 68.9, 110.8, 162.6 and 144.7 $Å^2$. The molecular weight and aLogP values are consistent with the Lipinski guidelines for orally available drugs (Lipinski et al., 2001). The topological polar surface areas are consistent with the complementary guidelines for oral availability proposed by Veber et al. (2002), with the exception of the class C compounds, which are above the recommended cutoff of 140 $Å^2$.

There are several prior reports on the physio-chemical and biological properties of the inhibitor scaffolds identified in this study. 8-Hydroxyquinolines (class A inhibitors) have been shown to have anti-bacterial (Darby et al., 2010) and anti-cancer activities (Jiang et al., 2011). Clioquinol (5-chloro-7-iodo-8-hydroxyquinoline) is an approved anti-fungal and anti-protozoal agent. PBT2, an analog of clioquinol, has shown efficacy in a transgenic mouse model of Alzheimer's disease (Adlard et al., 2008) and is in phase II clinical trials in humans (Lannfelt et al., 2008, Faux et al., 2010). Though 8-hydroxyquinolines are known metal-chelating compounds, some of the 8-alkoxyquinolines analogs studied here, which are unlikely to act as metal chelators, had strong inhibition potency. Also, $UTA1_{inh}$-A2 showed high UT-A1 selectivity over UT-B selectivity, suggesting a specific inhibition mechanism. Aminothiazolones (class B inhibitors) inhibit mushroom tyrosinase activity (Ha et al., 2012) and protect the liver in a concanavalin A-induced injury model (Luo et al., 2010). Dimeric aminothiazolone derivatives inhibit CDC25 phosphatases, which are involved in cell cycle progression and tumor development (Sarkis et al., 2012). Aminothiazolones are structurally similar to rhodanines, which are commonly identified from high-throughput screens, and have been considered promiscuous (Baell et al., 2010, Mendgen et al., 2012, Tomašić and Peterlin Mašič, 2012). This conclusion has been controversial, as potent and selective rhodanines are non-nucleoside inhibitors of hepatitis C NS5b RNA polymerase (Powers et al., 2006), and rosiglitazone and epalrestat, which are approved for anti-diabetes and diabetic neuropathy respectively, contain heterocycles similar to rhodanines and aminothiazolidones. Benzo-[1,3,5]-triazines (class C inhibitors) have been reported to have anti-cancer and antioxidant activities (Bekircan et al., 2005). Class D inhibitors are structural analogs of the triazolothienopyrimidine UTB_{inh}-14 that we previously reported as a UT-B-selective inhibitor (Anderson et al., 2012). This general scaffold has antagonist activity against 5-HT_6 receptors *in vitro* (Ivachtchenko et al., 2010). Synthesis of each of the four inhibitor classes can be accomplished in a modular manner, allowing diversification of the scaffold to improve physicochemical properties for follow-up medicinal chemistry.

UT-A1 inhibitors have a number of potential clinical indications. Urea transport inhibitors have a different mechanism-of-action from conventional diuretics, which block salt transport across kidney tubule epithelial cells. Conventional diuretics such as furosemide are used widely to increase renal salt and water clearance in conditions associated with total body fluid overload, including congestive heart failure, cirrhosis and nephrotic syndrome, as well in normovolemic states such as hypertension and syndrome of inappropriate secretion of

antidiuretic hormone (SIADH). By disrupting countercurrent mechanisms and intrarenal urea recycling, urea transport inhibitors, alone or in combination with conventional diuretics, may induce a diuresis in states of refractory edema where conventional diuretics are ineffective. Potential indications of urearetics include increasing solute clearance and free water excretion in states of fluid overload and hypertension. We note that the efficacy of urea transport inhibitors may be reduced in patients with low plasma urea concentrations and low rates of urea excretion, and when tubule function is impaired in acute or chronic renal insufficiency.

In summary, four chemical classes of drug-like UT-A1 inhibitors were identified, with analogs having a wide range of UT-A1 vs. UT-B selectivities. Functional studies and computational modeling identified putative inhibitor binding sites on the UT-A1 protein. Following optimization of pharmacological properties, to include selectivity studies against renal solute transporters, testing of inhibitors in rodent models of urinary concentrating function, edema and hypertension should be informative on the role of UT-A1 in normal physiology and edema states, and on the potential utility of UT-A1 inhibitors for drug therapy.

SIGNIFICANCE

Using a novel, target-based screening assay this study identified the first small-molecule UT-A1-selective inhibitors. UT-A1 inhibitors have applications in elucidating the physiological role of urea transport in the urinary concentrating mechanism, and are potential drug development candidates predicted to have therapeutic efficacy as ‘urearetics’ in states of refractory edema, as in congestive heart failure and cirrhosis, in which conventional salt transport-blocking diuretics such as furosemide have limited efficacy. UT-A1 inhibitors would be first-in-their class drugs that address an unmet need in kidney drug therapy.

EXPERIMENTAL PROCEDURES

Collection of rat blood

Whole blood was collected from 12–16 week-old (300–400 g) Wistar rats by orbital puncture after subcutaneous injection of sodium heparin. Procedures were approved by the Committee on Animal Research at the University of California, San Francisco.

Cell lines

MDCK cells stably transfected with rat UT-A1 (MDCK-UT-A1, Froehlich et al., 2006) were grown in Dulbecco’s modified Eagle medium (DMEM) containing 10% FBS, penicillin G (100 U/ml), streptomycin (100 μg/ml) and hygromycin (500 μg/ml). The cells were co-transfected with yellow fluorescent protein YFP-H148Q/V163S (Galietta et al., 2001) using Lipofectamine 2000 (Invitrogen, Carlsbad, CA) according to the manufacturer’s instructions. Cells resistant to hygromycin (500 μg/ml) and G418 (600 μg/ml) were selected by flow cytometry. The UT-A1/YFP-transfected cells were then transfected with cDNA encoding AQP1 and selected with Zeocin (500 μg/ml). MDCK cells were maintained in DMEM supplemented with 10% FBS, penicillin G (100 U/ml) and streptomycin (100 μg/ml) at 37 °C, 5% CO_2.

Immunofluorescence

Transfected MDCK cells were seeded onto poly-D-lysine-coated, 12-mm diameter coverslips and fixed with 4% paraformaldehyde for 15 min. After blocking and permeabilization with 1% bovine serum albumin and 0.1% Triton X-100 for 30 min,

coverslips were incubated with mouse anti-AQP1 (1:100, Santa Cruz Biotechnology, Inc., Santa Cruz, CA) and rabbit anti-UT-A1 (1: 1000, LifeSpan BioSciences, Inc., Seattle, WA) for 2 h. Cells were then rinsed extensively with PBS and incubated for 60 min with 4 μg/mL donkey anti-mouse IgG-conjugated Alexa Fluor 555 and goat anti-rabbit IgG-conjugated Alexa Fluor 647 (Invitrogen, Carlsbad, CA). Cells were imaged using a laser scanning confocal microscope D-Eclipse C1 (Nikon) equipped with a Nikon 100×, NA 1.49 Apo lens.

UT-A1 inhibitor identification by high-throughput screening

Primary screening was done using a collection of 90,320 diverse, drug-like compounds from ChemDiv (San Diego, CA). For analysis of structure-activity relationships, >400 commercially available analogs (ChemDiv and Asinex) were tested. Cells were plated into black 96-well microplates with clear plastic bottoms (Corning-Costar 3904) at 15,000 cells/well and cultured for 24 h at 37 °C before assay. Microplates containing cultured cells were washed twice with PBS and 150 μL of test compound (25 μM final) was added and incubated at 37°C, 90% humidity, 5% CO_2 for 15 min. Eighty wells contained test compounds, and the first and last columns of each plate were used for negative (no test compound) and positive (0.35 mM phloretin) controls. Assays were done on a plate reader (Tecan Trading AG, Switzerland) equipped with custom YFP filter set. Each assay consisted of a continuous 15-s read (5 Hz) with 50 μL of 3.2 M urea in PBS injected at 1 s (at 130 μL/sec) to give a 800 mM final urea gradient. Initial rates of urea influx were computed using a model of cell shrinking-swelling described previously (Levin et al., 2007) and analyzed using GraphPad Prism, version 5.01.

Functional characterization of UT-A1 inhibitors

Reversibility of UT-A1 inhibition was tested by pre-incubating MDCK cells (expressing YFP-H148Q/V163S, AQP1 and UT-A1) with inhibitors for 15 min (at 3 μM) and then washing with PBS prior to assay. The urea concentration dependence of UT-A1 inhibition was studied from inhibitor concentration-response data (0.3–60 μM) using different of urea gradients (200–1,600 mM). The kinetics of UT-A1 inhibition was measured by adding inhibitors (3 μM) at different times prior to assay.

UT-B inhibition measurements

Whole rat blood was diluted to a hematocrit of ~1.6% in PBS containing 1.25 M acetamide and 5 mM glucose. 100 μL of the erythrocyte suspension was added to each well of a 96-well round-bottom microplate, to which test compounds were added. After 15 min incubation, 20 μL of the erythrocyte suspension was added rapidly to each well of a 96-well black-walled plate containing 180 μL PBS containing 1% DMSO. Vigorous mixing was achieved by repeated pipetting. Erythrocyte lysis was quantified by absorbance at a 710-nm wavelength. No-lysis controls (isotonic buffer; PBS plus 1.25 M acetamide with 1% DMSO) and full-lysis controls (distilled H_2O) were done in all plates. Percentage erythrocyte lysis was computed as: % lysis = 100% $(A_{neg} - A_{test})/(A_{neg} - A_{pos})$, where A are absorbance values at 710 nm.

Transepithelial transport measurements

MDCK-UT-A1 cells were grown on 12-mm diameter collagen-coated Transwell inserts (0.4 μm pore size; Costar) as described (Levin et al., 2007). Inserts were loaded with 2×10^5 cells/cm^2 and cultured for 4 days to form tight monolayers with transepithelial resistance 500–600 Ω cm^2. Urea flux in the basolateral-to-apical direction was measured in response to a 15 mM urea gradient. Measurements were done in 12-well plates in which PBS, containing either DMSO vehicle or forskolin (10 μM), with or without UT-A1 inhibitor, was added to both the apical-facing (0.2 ml) and basal-facing (1 ml) surfaces. Cultures were

incubated for 30 min at 37 °C, then the basal-facing solution was replaced by PBS (containing the same components) plus 15 mM urea. Samples (5 μl) of apical fluid were collected at specified times for urea assay (Quantichrom Urea Assay Kit, BioAssay Systems, Hayward, CA). Inhibition was computed as *% inhibition* = 100%·(A_{forsk}−A_{test})/(A_{forsk}−A_{phlor}). A_{forsk} and A_{phlor} are absorbance (at 520 nm) for cultures treated with forskolin and forskolin + phloretin, respectively, and A_{test} from cultures treated with forskolin + test compound.

Homology modeling and docking computations

A homology model of human UT-A1 was generated using the SWISS MODEL online utility (http://swissmodel.expasy.org) in automated mode, using the sequence of the full rat UT-A1 protein (accession code, NP_062220.2). The model was generated using coordinates from the X-ray crystal structure of bovine UT-B (PDB=4EZC, solved to 2.5 Å) (Levin et al., 2012) as a homology template. Two structural models were generated, comprising residues 105–449 (65.2% identity with bovine UT-B) and 568–909 of UT-A1 (67.5% sequence identity with bovine UT-B). Due to the slightly improved sequence identity, the latter model was used for docking computations. Because the UT-B structure was solved as a trimer of identical structures, the homology model was also generated in this format, and a single structure of the UT-A1 model was isolated for docking computations. The homology model of UT-A1 was prepared for docking using the FRED-RECEPTOR utility (OpenEye Scientific, Santa Fe, NM), with cytoplasmic and extracellular domains defined with 10 cubic Å boxes. Structures of class A, B and C inhibitors were drawn in ChemDraw (Cambridge Software, Cambridge, MA), converted to SMILES strings, transformed to three-dimensional conformations, and minimized using PIPELINE PILOT (Accelrys, San Diego, CA). The single conformations were passed through MOLCHARGE (OpenEye Scientific, Santa Fe, NM) to apply MMFF charges, and through OMEGA (OpenEye Scientific) to generate multi-conformational libraries. The inhibitor conformational libraries were docked using FRED (v2.2.5) (OpenEye Scientific), which was configured to use consensus scoring functions ChemGauss3, ChemScore, OEChemScore, ScreenScore, ShapeGauss, PLP, and ZapBind. Docking of the inhibitors was carried out free of pharmacophore restraint. The final protein-inhibitor complexes were visualized using PYMOL (Schrödinger, San Diego, CA).

Acknowledgments

This study was supported by grants DK35124, DK72517, DK86125, EB00415 and EY13574 from the National Institutes of Health and a grant from the Fulbright Program and the Ministry of Education, Culture and Sports of Spain.

References

Anderson MO, Zhang J, Liu Y, Yao C, Phuan PW, Verkman AS. Nanomolar potency and metabolically stable inhibitors of kidney urea transporter UT-B. J Med Chem. 2012; 55:5942–5950. [PubMed: 22694147]

Adlard PA, Cherny RA, Finkelstein DI, Gautier E, Robb E, Cortes M, Volitakis I, Liu X, Smith JP, Perez K, Laughton K, Li QX, Charman SA, Nicolazzo JA, Wilkins S, Deleva K, Lynch T, Kok G, Ritchie CW, Tanzi RE, Cappai R, Masters CL, Barnham KJ, Bush AI. Rapid restoration of cognition in Alzheimer's transgenic mice with 8-hydroxy quinoline analogs is associated with decreased interstitial Abeta. Neuron. 2008; 59:43–55. [PubMed: 18614028]

Baell JB, Holloway GA. New substructure filters for removal of pan assay interference compounds (PAINS) from screening libraries and for their exclusion in bioassays. J Med Chem. 2010; 53:2719–2740.

Bagnasco SM. Gene structure of urea transporters. Am J Physiol Renal Physiol. 2003; 284:F3–F10.

Bankir L, Yang B. New insights into urea and glucose handling by the kidney, and the urine concentrating mechanism. Kidney Internat. 2012; 81:1179–1198.

Bekircan O, Küxük M, Kahveci B, Kolayli S. Convenient synthesis of fused heterocyclic 1,3,5-triazines from some N-acyl imidates and heterocyclic amines as anticancer and antioxidant agents. Arch Pharm (Weinheim). 2005; 338:365–372. [PubMed: 16041836]

Darby CM, Nathan CF. Killing of non-replicating Mycobacterium tuberculosis by 8-hydroxyquinoline. J Antimicrob Chemother. 2010; 65:1424–1427. [PubMed: 20435781]

Doran JJ, Klein JD, Kim YH, Smith TD, Kozlowski SD, Gunn RB, Sands JM. Tissue distribution of UT-A and UT-B mRNA and protein in rat. Am J Physiol Regul Integr Comp Physiol. 2006; 290:R1446–R1459. [PubMed: 16373440]

Faux NG, Ritchie CW, Gunn A, Rembach A, Tsatsanis A, Bedo J, Harrison J, Lannfelt L, Blennow K, Zetterberg H, Ingelsson M, Masters CL, Tanzi RE, Cummings JL, Herd CM, Bush AI. PBT2 rapidly improves cognition in Alzheimer's Disease: additional phase II analyses. J Alzheimers Dis. 2010; 20:509–516. [PubMed: 20164561]

Fenton RA, Stewart GS, Carpenter B, Howorth A, Potter EA, Cooper GJ, Smith CP. Characterization of mouse urea transporters UT-A1 and UT-A2. Am J Physiol Renal Physiol. 2002; 283:F817–825.

Fenton RA, Chou CL, Stewart GS, Smith CP, Knepper MA. Urinary concentrating defect in mice with selective deletion of phloretin-sensitive urea transporters in the renal collecting duct. Proc Natl Acad Sci USA. 2004; 101:7469–7474. [PubMed: 15123796]

Fenton RA, Flynn A, Shodeinde A, Smith CP, Schnermann J, Knepper MA. Renal phenotype of UT-A urea transporter knockout mice. J Am Soc Nephrol. 2005; 16:1583–1592. [PubMed: 15829709]

Fenton RA. Urea transporters and renal function: lessons from knockout mice. Curr Opin Nephrol Hypertens. 2008; 17:513–518. [PubMed: 18695393]

Fenton RA. Essential role of vasopressin-regulated urea transport processes in the mammalian kidney. Pflugers Arch. 2009; 458:169–177. [PubMed: 19011892]

Frohlich O, Klein JD, Smith PM, Sands JM, Gunn RB. Regulation of UT-A1-mediated transepithelial urea flux in MDCK cells. Am J Physiol Cell Physiol. 2006; 291:C600–D606. [PubMed: 16641165]

Galietta LJ, Haggie PM, Verkman AS. Green fluorescent protein-based halide indicators with improved chloride and iodide affinities. FEBS Lett. 2001; 499:220–224. [PubMed: 11423120]

Ha YM, Park YJ, Kim JA, Park D, Park JY, Lee HJ, Lee JY, Moon HR, Chung HY. Design and synthesis of 5-(substituted benzylidene)thiazolidine-2,4-dione derivatives as novel tyrosinase inhibitors. Eur J Med Chem. 2012; 49:245–252. [PubMed: 22301213]

Ivachtchenko AV, Golovina ES, Kadieva MG, Koryakova AG, Kovalenko SM, Mitkin OD, Okun IM, Ravnyeyko IM, Tkachenko SE, Zaremba OV. Synthesis and biological study of 3-(phenylsulfonyl)thieno[2,3-e][1,2,3]triazolo[1,5-a]pyrimidines as potent and selective serotonin 5-HT6 receptor antagonists. Bioorg Med Chem. 2010; 18:5282–5290. [PubMed: 20541425]

Jiang H, Taggart JE, Zhang X, Benbrook DM, Lind SE, Ding WQ. Nitroxoline (8-hydroxy-5-nitroquinoline) is more a potent anti-cancer agent than clioquinol (5-chloro-7-iodo-8-quinoline). Cancer Lett. 2011; 312:11–17.

Klein JD, Blount MA, Sands JM. Molecular mechanisms of urea transport in health and disease. Pflugers Arch. 2012; 464:561–572. [PubMed: 23007461]

Klein JD, Frohlich O, Mistry AC, Kent KJ, Martin CF, Sands JM. Transgenic mice expressing UT-A1, but lacking UT-A3, have intact urine concentration ability. FASEB J. 2013; 27:1111.17. (Experimental Biology abstract).

Lannfelt L, Blennow K, Zetterberg H, Batsman S, Ames D, Harrison J, Masters CL, Targum S, Bush AI, Murdoch R, Wilson J, Ritchie CW. Safety, efficacy, and biomarker findings of PBT2 in targeting Abeta as a modifying therapy for Alzheimer's disease: a phase IIa, double-blind, randomised, placebo-controlled trial. Lancet Neurol. 2008; 7:779–786. [PubMed: 18672400]

Lei T, Zhou L, Layton AT, Zhou H, Zhao X, Bankir L, Yang B. Role of thin descending limb urea transport in renal urea handling and the urine concentrating mechanism. Am J Physiol Renal Physiol. 2011; 301:F1251–F1259. [PubMed: 21849488]

Levin EJ, Cao Y, Enkavi G, Quick M, Pan Y, Tajkhorshid E, Zhou M. Structure and permeation mechanism of a mammalian urea transporter. Proc Natl Acad Sci USA. 2012; 109:11194–11199. [PubMed: 22733730]

Levin MH, de la Fuente R, Verkman AS. Urearetics: a small molecule screen yields nanomolar potency inhibitors of urea transporter UT-B. FASEB J. 2007; 21:551–563. [PubMed: 17202246]

Li F, Lei T, Zhu J, Wang W, Sun Y, Chen J, Dong Z, Zhou H, Yang B. A novel small-molecule thienoquinolin urea transporter inhibitor acts as a potential diuretic. Kidney Int. 2013; 83:1076–1086. [PubMed: 23486518]

Lipinski CA, Lombardo F, Dominy BW, Feeney PJ. Experimental and computational approaches to estimate solubility and permeability in drug discovery and development settings. Adv Drug Deliv Rev. 2001; 46:3–26. [PubMed: 11259830]

Lucien N, Sidoux-Walter F, Olives B, Moulds J, Le Pennec PY, Cartron JP, Bailly P. Characterization of the gene encoding the human Kidd blood group/urea transporter protein. Evidence for splice site mutations in Jknull individuals. J Biol Chem. 1998; 273:12973–12980. [PubMed: 9582331]

Luo Y, Ma L, Zheng H, Chen L, Li R, He C, Yang S, Ye X, Chen Z, Li Z, Gao Y, Han J, He G, Yang L, Wei Y. Discovery of (Z)-5-(4-methoxybenzylidene)thiazolidine-2,4-dione, a readily available and orally active glitazone for the treatment of concanavalin A-induced acute liver injury of BALB/c mice. J Med Chem. 2010; 53:273–281. [PubMed: 19904929]

Mayrand RR, Levitt DG. Urea and ethylene glycol-facilitated transport systems in the human red cell membrane. Saturation, competition, and asymmetry. J Gen Physiol. 1983; 81:221–237. [PubMed: 6842173]

Mendgen T, Steuer C, Klein CD. Privileged scaffolds or promiscuous binders: a comparative study on rhodanines and related heterocycles in medicinal chemistry. J Med Chem. 2012; 55:743–753. [PubMed: 22077389]

McGann M. FRED pose prediction and virtual screening accuracy. J Chem Inf Model. 2011; 51:578–596. [PubMed: 21323318]

Pannabecker TL. Comparative physiology and architecture associated with the mammalian urine concentrating mechanism: role of inner medullary water and urea transport pathways in the rodent medulla. Am J Physiol Regul Integr Comp Physiol. 2013; 304:R488–503. [PubMed: 23364530]

Powers JP, Piper DE, Li Y, Mayorga V, Anzola J, Chen JM, Jaen JC, Lee G, Liu J, Peterson MG, Tonn GR, Ye Q, Walker NP, Wang Z. SAR and mode of action of novel non-nucleoside inhibitors of hepatitis C NS5b RNA polymerase. J Med Chem. 2006; 49:1034–1046. [PubMed: 16451069]

Sands JM, Gargus JJ, Frohlich O, Gunn RB, Kokko JP. Urinary concentrating ability in patients with Jk(a-b-) blood type who lack carrier-mediated urea transport. J Am Soc Nephrol. 1992; 2:1689–1696. [PubMed: 1498276]

Sands JM. Renal urea transporters. Curr Opin Nephrol Hypertens. 2004; 13:525–532. [PubMed: 15300159]

Sands JM. Critical role of urea in the urine-concentrating mechanism. J Am Soc Nephrol. 2007; 18:670–671. [PubMed: 17251382]

Sands JM, Layton HE. The physiology of urinary concentration: an update. Semin Nephrol. 2009; 29:178–195. [PubMed: 19523568]

Sarkis M, Tran DN, Kolb S, Miteva MA, Villoutreix BO, Garbay C, Braud E. Design and synthesis of novel bis-thiazolone derivatives as micromolar CDC25 phosphatase inhibitors: effect of dimerisation on phosphatase inhibition. Bioorg Med Chem Lett. 2012; 24:7345–7350.

Shayakul C, Hediger MA. The SLC14 gene family of urea transporters. Pflugers Arch. 2004; 447:603–609. [PubMed: 12856182]

Shayakul C, Clémençon B, Hediger MA. The urea transporter family (SLC14): physiological, pathological and structural aspects. Mol Aspects Med. 2013; 34:313–322.

Smith CP. Mammalian urea transporters. Exp Physiol. 2009; 94:180–185.

Stewart G. The emerging physiological roles of the SLC14A family of urea transporters. Br J Pharmacol. 2011; 164:1780–1792.

Tomašić T, Peterlin Mašič L. Rhodanine as a scaffold in drug discovery: a critical review of its biological activities and mechanisms of target modulation. Expert Opin Drug Discov. 2012; 7:549–560.

Tsukaguchi H, Shayakul C, Berger UV, Tokui T, Brown D, Hediger MA. Cloning and characterization of the urea transporter UT3: localization in rat kidney and testis. J Clin Invest. 1997; 99:1506–1515.

Uchida S, Sohara E, Rai T, Ikawa M, Okabe M, Sasaki S. Impaired urea accumulation in the inner medulla of mice lacking the urea transporter UT-A2. Mol Cell Biol. 2005; 25:7357–7363.

Veber DF, Johnson SR, Cheng HY, Smith BR, Ward KW, Kopple KD. Molecular properties that influence the oral bioavailability of drug candidates. J Med Chem. 2002; 45:2616–2623.

Yang B, Bankir L, Gillespie A, Epstein CJ, Verkman AS. Urea-selective concentrating defect in transgenic mice lacking urea transporter UT-B. J Biol Chem. 2002; 277:10633–10637.

Yang B, Verkman AS. Analysis of double knockout mice lacking aquaporin-1 and urea transporter UT-B. Evidence for UT-B-facilitated water transport in erythrocytes. J Biol Chem. 2002; 277:36782–36786. [PubMed: 12133842]

Yao C, Anderson MO, Zhang J, Yang B, Phuan PW, Verkman AS. Triazolothienopyrimidine inhibitors of urea transporter UT-B reduce urine concentration. J Am Soc Nephrol. 2012; 23:1210–1220. [PubMed: 22491419]

HIGHLIGHTS

- U T-A1 screen assay was established using fluorescent, UT-A1-expressing MDCK cells.
- 4 UT-A1 inhibitor classes were identified with different UT-A1/UT-B selectivity.
- Functional studies showed a reversible, non-competitive binding mechanism.
- Computational studies suggested inhibitor binding in the UT-A1 hydrophobic pore.

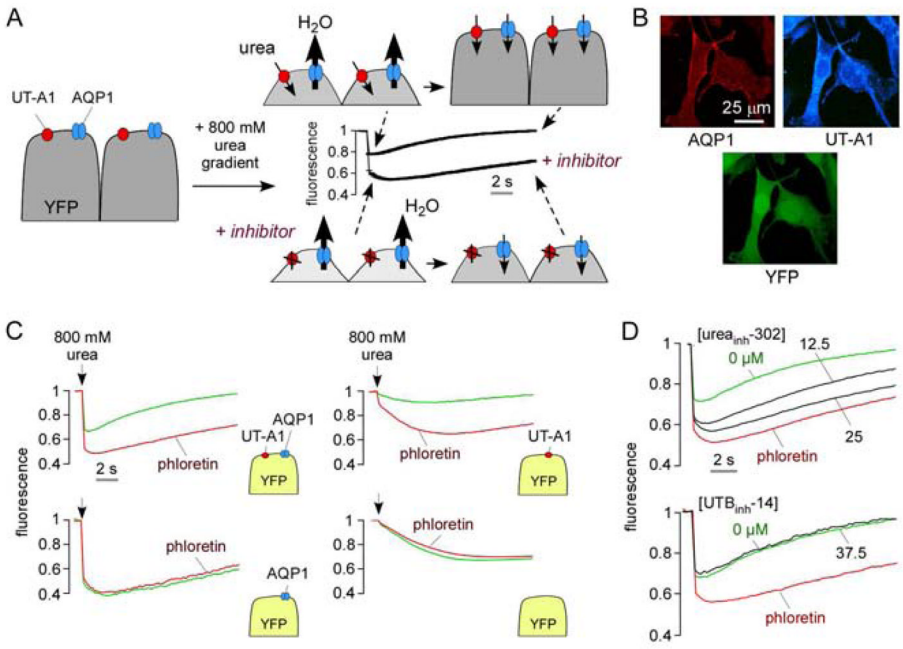

Figure 1. Development and validation of UT-A1 inhibitor screen

A. Assay method. MDCK cells stably expressing UT-A1, AQP1 and YFP-H148Q/V163S are subjected to a 800-mM urea gradient. A rapid decrease of the cell volume (reduced fluorescence) due to the water efflux through AQP1 is followed by cell re-swelling (increased fluorescence) due to urea and water. The UT-A1 inhibitor phloretin alters curve shape. **B.** UT-A1 and AQP1 immunofluorescence of the triply transfected cells, shown with YFP fluorescence. **C.** YFP fluorescence kinetics in response to an 800-mM urea gradient in cells expressing YFP-H148Q/V163S alone and together with UT-A1 and/or AQP1. **D.** Effects of prior UT-B inhibitors $urea_{inh}$-302 (Levin et al., 2007) and UTB_{inh}-14 (Yao et al., 2012) on UT-A1 urea transport. In this and subsequent data curves shown in green and red represent control (no inhibitor) and full inhibition (phloretin), respectively.

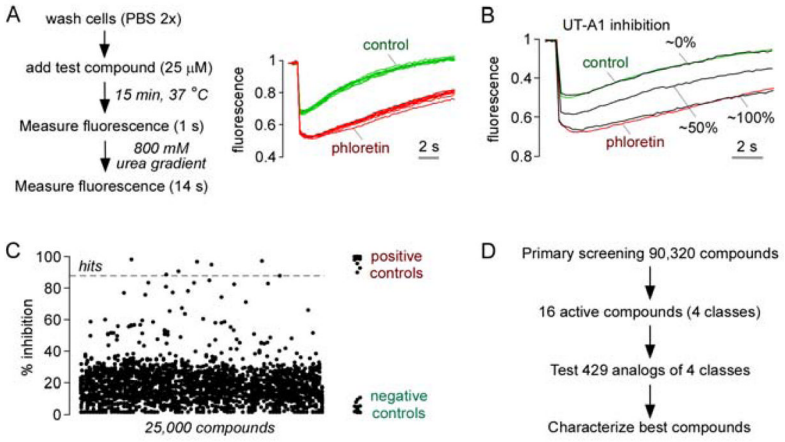

Figure 2. UT-A1 inhibitor identification by high-throughout screening

A. Screening assay (left). YFP fluorescence curves from 10 negative (vehicle control) and 10 positive (full inhibition with phloretin) wells (right). **B.** Examples of compounds from primary screening showing ~0%, 50% and 100 % inhibition of UT-A1 urea transport. **C.** Summary of percentage UT-A1 inhibition by 25,000 compounds from the primary screen. Twenty replicates of negative and positive controls shown at the right. **D.** Summary of findings of the primary screen.

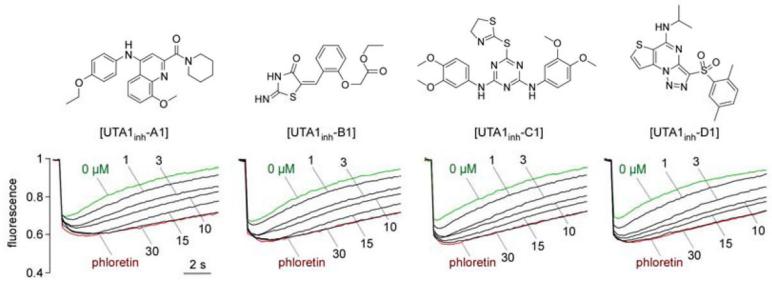

Figure 3. UT-A1 inhibitors identified in the screen

Chemical structures of UT-A1 inhibitors ($UTA1_{inh}$-xx, with xx the identifying code) of each of four chemical classes (top). Concentration-inhibition data for each inhibitor (bottom).

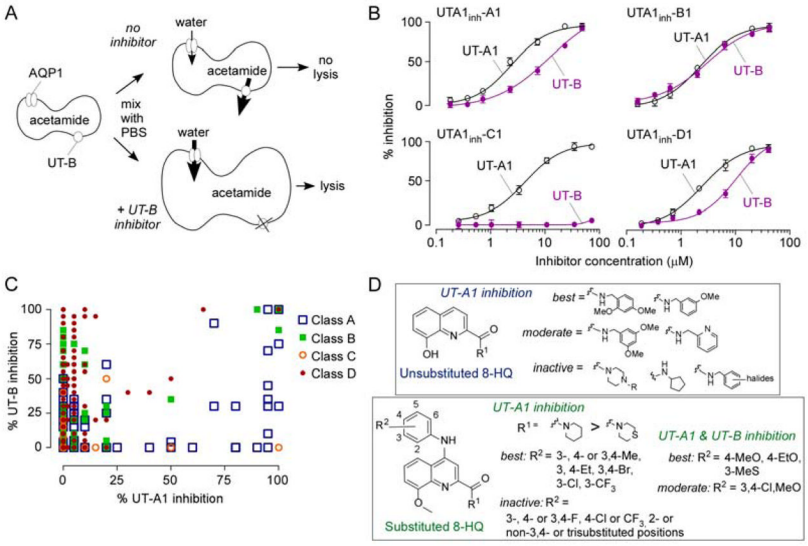

Figure 4. Selectivity and structure-activity analysis of UT-A1 inhibitors

A. UT-B inhibition assay showing rapid dilution of acetamide-loaded rat erythrocytes in acetamide-free PBS, resulting in osmotic cell swelling after UT-B–facilitated acetamide efflux and consequent cell shrinking. UT-B inhibition allows unopposed cell swelling and causes erythrocyte lysis. **B.** Concentration-inhibition data for inhibition of UT-A1 and UT-B for the four compounds from Fig. 3 (Mean ± SEM). **C.** Percentage UT-B (y-axis) and UT-A1 (x-axis) inhibition for selected class A, B, C and D compounds tested at 25 μM. **D.** (top) Structural determinants of unsubstituted 8-hydroxyquinolines (8-HQ) for UT-A1 inhibition activity. (bottom) Structural determinants of aniline-substituted 8-HQ for selective UT-A1 and dual UT-A1 and UT-B inhibition activities.

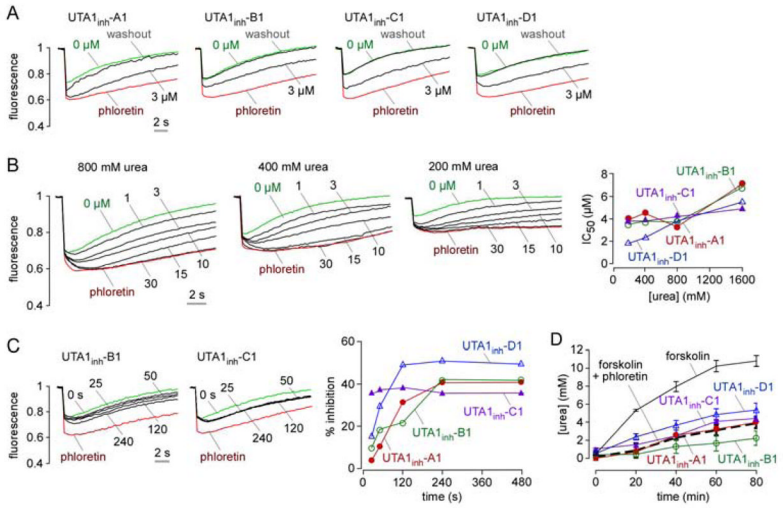

Figure 5. Characterization of UT-A1 inhibitors

A. Reversibility. Compounds were incubated (at 3 μM) with the triple transfected MDCK cells for 15 min, then washed twice and subjected to UT-A1 inhibition assay. **B.** Urea competition. Concentration-inhibition data for $UTA1_{inh}$-A1 using 800, 400 and 200-mM urea gradients (left). Summary of IC_{50} as a function of urea gradient (right). **C.** Kinetics of UT-A1 inhibition. UT-A1 urea transport measured at different times after addition of 3 μM $UTA1_{inh}$-B1 or $UTA1_{inh}$-C1 (left). Deduced time course of percentage inhibition of UT-A1 urea transport (right). **D.** Transepithelial urea transport in MDCK cells stably expressing UT-A1. Cells were treated with 10 μM forskolin alone (black), forskolin + phloretin (0.7 mM) (dashed thick black) and forskolin plus each of the indicated UT-A1 inhibitors at 30 μM (Mean ± SEM).

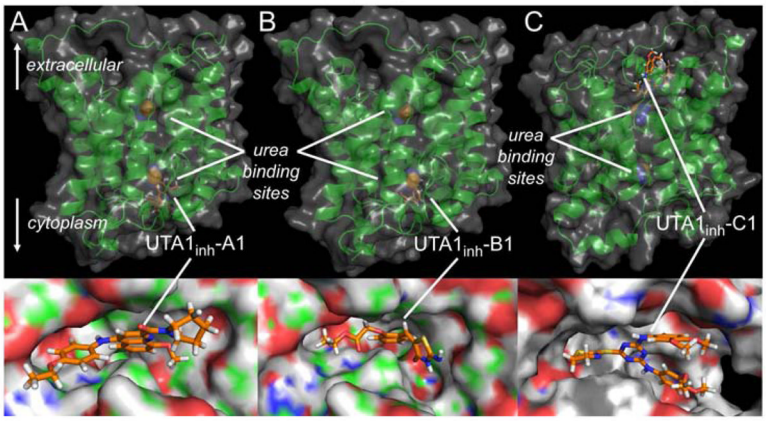

Figure 6. Computational modeling of urea transporter – inhibitor interaction

Putative inhibitor binding sites in rat UT-A1 deduced by functional measurements, homology modeling, and computational docking. Zoomed-in and zoomed-out representations of representations of $UTA1_{inh}$-A1 (**A**) and $UTA1_{inh}$-B1 (**B**) bound to the UT-A1 cytoplasmic domain; and $UTA1_{inh}$-C1 (**C**) bound to the extracellular domain. Positions of putative urea binding sites deduced from homology modeling are indicated.

Table 1

Structure-activity analysis of urea transport inhibition

Potency and UT-A1 and UT-B selectivity of selected analogs from each of the four structural class of urea transport inhibitors were examined.

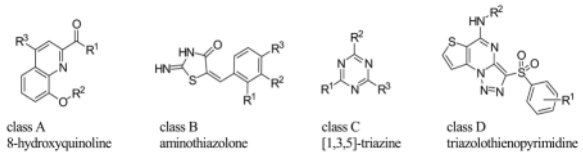

Class	Inhibitor	R^1	R^2	R^3	UT-A1 IC_{50} (μM)	UT-B IC_{50} (μM)
A	$UTA1_{inh}$-A1	piperidine	Me	4-EtO-aniline	3.3	16
	$UTA1_{inh}$-A2	3-MeO-benzylamine	H	H	5.3	>50
	$UTA1_{inh}$-A3	thiomorpholine	Me	4-MeO-aniline	3.5	6.2
	$UTA1_{inh}$-A4	piperidine	Me	3-MeS-aniline	3.8	20
	$UTA1_{inh}$-A5	thiomorpholine	Me	4-EtO-aniline	24	34
	$UTA1_{inh}$-A6	thiomorpholine	Me	3-Cl,4-MeO-aniline	19	27
	$UTA1_{inh}$-A7	piperidine	Me	3-Cl,4-Me-aniline	24	>50
	$UTA1_{inh}$-A8	piperidine	Me	3-F,4-Me-aniline	25	>50
B	$UTA1_{inh}$-B1	O-ethyl acetate	H	H	3.7	4.8
	$UTA1_{inh}$-B2	OH	OMe	H	4.6	6.3
	$UTA1_{inh}$-B3	OMe	OMe	H	7.0	43
	$UTA1_{inh}$-B4	H	OMe	OH	25	6.2
C	$UTA1_{inh}$-C1	3,4-MeO-aniline	2-thio(4,5-dihydro-thiazole)	3,4-MeO-aniline	4.2	>50
	$UTA1_{inh}$-C2	MeS	4-NH-Phenyl-aniline	MeS	45	>50
	$UTA1_{inh}$-C3	3-MeO-aniline	4-Me-thiophenol	4-Me-aniline	>50	42
D	$UTA1_{inh}$-D1	2,5-Me	isopropyl		3.8	15
	$UTA1_{inh}$-D2	unsubstituted	Me		>50	35
	$UTA1_{inh}$-D3	4-Br	thiophene		>50	2.8
	$UTA1_{inh}$-D4	4-Et	3-MeO-propyl		>50	28

Chem Biol. Author manuscript; available in PMC 2014 October 24.